Fam, M. & Santamarina, J. C. (1997). *Géotechnique* **47**, No. 2, 203–219

A study of consolidation using mechanical and electromagnetic waves

M. FAM* and J. C. SANTAMARINA†

Consolidation has been a central topic of research in geotechnical engineering. Most studies have been conducted in oedometric cells, and have attempted to assess the influence of multiple material and loading parameters. Yet, the characterization of internal processes and the role of mechanical and electrical interparticle forces still remains elusive. In this study, we monitored the consolidation of bentonite, kaolinite and silica flour with small-perturbation electromagnetic and mechanical waves. The resulting standard consolidation test data, and the simultaneously acquired wave data are presented. Macro-observations are interpreted at the micro-level. Changes in the high-frequency complex dielectric permittivity during the consolidation of kaolinite indicate a decrease in free water inside the specimen, and no changes in double-layer polarizability. The velocity of propagation of shear waves clearly reflects the transfer of load from pore pressure to skeletal stresses, and the corresponding increase in stiffness during consolidation. Velocity–stress relationships reflect contact behaviour, changes in mechanical and electrostatic interparticle forces and modifications in microfabric. The small-strain shear stiffness drops immediately on loading because of spatial variations in pore pressure; the time required to recover the initial stiffness depends on soil permeability. Results indicate the potential for development of innovative wave-based monitoring techniques for field applications.

KEYWORDS: clays; consolidation; laboratory tests; monitoring; stiffness; waves and wave loading.

Les recherches sur la consolidation ont une importance majeure en génie géotechnique. La plupart des études reposent sur l'emploi d'oedomètres et visent à évaluer l'influence des matériaux et des charges dans une multiplicité de paramètres. Toutefois, il reste difficile de caractériser les processus internes et le rôle des forces mécaniques et électriques entre les particules. Dans notre étude, nous avons observé la consolidation de bentonite, de kaolinite et de poudre de silice sous l'effet de petites ondes de perturbation électromagnétiques et mécaniques. Nous présentons les résultats d'essais standard de consolidation et les données relevées parallèlement sur les ondes. Les macro-observations font l'objet d'une micro-interprétation. Les variations de permittivité diélectrique complexe hautes fréquences pendant la consolidation de la kaolinite indiquent une diminution d'eau gravitaire dans l'éprouvette, mais aucun changement de la polarisabilité en deux couches. La vitesse de propagation des ondes de cisaillement révèle clairement que la pression interstitielle se transforme en tensions qui viennent solliciter le squelette et que la rigidité augmente de façon correspondante pendant la consolidation. Les rapports vitesse–contrainte expriment le comportement de contact, le changement des forces mécaniques et électrostatiques entre les particules, et les modifications de la microstructure. La résistance aux petites déformations de cisaillement chute immédiatement au chargement en raison des variations spatiales de la pression interstitielle. Le temps nécessaire pour retourner à la rigidité initiale dépend de la perméabilité du sol. Les résultats donnent à penser qu'il y aurait lieu de mettre au point des techniques novatrices de contrôle de la consolidation basées sur la propagation des ondes, qui puissent être appliquées sur le terrain.

Manuscript received 3 January 1995; revised manuscript accepted 13 March 1996.
Discussion on this paper closes 1 September 1997; for further details see p. ii.
* University of Waterloo, Canada.
† Georgia Institute of Technology, Atlanta; formerly at University of Waterloo, Canada.

INTRODUCTION

Consolidation is the time-dependent decrease in volume of saturated soils subjected to loading. This phenomenon has been extensively studied since the 1920s when Terzaghi postulated the effective stress principle. Consolidation is the combination of two coupled phenomena: permeability, which controls

the rate of water flow, and compressibility of the soil fabric, which controls the change in volume for a given change in load. Within the timing of civil engineering events, consolidation is most relevant in clayey soils. Furthermore, clays present unique phenomena owing to the co-participation of mechanical–gravimetric and electrical interparticle forces and the formation of double layers.

Different methodologies have been adopted to study consolidation. These include testing with varied boundary conditions, measuring the effect of different sample height/diameter ratios, investigating the significance of pore fluid changes and altering loading rates (e.g. Olsen & Ladd, 1979). Several theories have been developed to interpret test results, such as non-linear stress–strain relationships, layered systems, large strains, coupled gradients and the modified effective stress concept.

Wave propagation is a small perturbation, which permits monitoring on-going processes without causing permanent disturbance. Electromagnetic and mechanical waves provide complementary information. Electromagnetic wave propagation is influenced by the ability to displace charges or to rotate dipoles. On the other hand, the propagation of mechanical waves through particulate geomaterials is influenced by the nature of contact rigidity and by interparticle forces. The interaction of both electromagnetic and mechanical waves with any material is characterized by two parameters: real and imaginary permittivity in the case of electromagnetic waves, and velocity and attenuation in the case of mechanical waves. These parameters are frequency dependent.

The experimental study discussed in this paper applies wave propagation techniques to monitor consolidation; both mechanical and electromagnetic waves are used. The purpose of this paper is twofold: to provide further insight into the phenomenon of consolidation, through wave propagation, and, conversely, to develop an enhanced understanding of wave–geomedia interaction within the context of a well-studied macro-phenomenon, in a well-controlled experimental setting. This paper starts with a summary of fundamental concepts related to wave–geomedia interaction.

FUNDAMENTAL CONCEPTS

Electromagnetic waves—complex permittivity

The increase in the surface charge of a capacitor just after inserting a dielectric material between its electrodes reflects the polarization of the material. In materials with dipolar molecules, polarization is defined as the number of dipole moments oriented in the field direction per unit volume. There are different polarization mechanisms that are responsible for this phenomenon (Santamarina & Fam, 1997). Water is a dipolar molecule, and it therefore exhibits orientational polarization in the GHz frequency range (Debye, 1929). The fact that soils are heterogeneous mixtures adds another polarization mechanism, Maxwell–Wagner spatial polarization, which arises because of differences in conductivity and permittivity of the constituents. In addition, double layers polarize owing to the displacement of the positive ionic cloud with respect to the negative clay particle on the application of an electric field. Double-layer and spatial polarization relaxation occur at kHz or MHz frequencies. The imaginary permittivity expresses two types of losses: polarization losses and conductivity losses. Each polarization mechanism is accompanied by an increase in polarization losses, while increased ionic concentration and mobility increase the contribution of ohmic losses (Jonscher, 1983; Dukhin & Shilov, 1973; Hasted, 1973, Hill *et al*., 1969; DeLoor, 1968; von Hippel, 1954; Debye, 1929).

Water content—dielectric permittivity

The real permittivity of soils at GHz frequencies, κ', reflects the amount of free water (mineral powders, $\kappa' \approx 6$; free water, $\kappa' \approx 80$; adsorbed water, $\kappa' \approx 3$). However, at low frequencies, spatial and double layer polarizations add to the permittivity (Okonski, 1960; Schwarz, 1962; Schurr, 1964; Lyklema *et al*., 1983). Permittivity is governed by the volumetric water content w_{vol} rather than the gravimetric water content (Selig & Manuskhani, 1975; Dobson & Ulaby, 1981):

$$w_{vol} = V_w / V_t \tag{1}$$

where V_w is the volume of the water phase and V_t is the total volume of the soil.

Soil permittivity increases slowly at low volumetric moisture content. After reaching a transition moisture content (not necessarily well defined), permittivity increases steeply (Wang & Schmugge, 1980).

Theoretical and empirical mixing models can be used to predict the permittivity of a soil mixture as a function of the permittivity of its constituents. Such models can be used to estimate the moisture content of different soil strata from wave data (Smith *et al*., 1992). Some of these models consider bound water in the vicinity of the clay particle: since water molecules in this region are influenced by the electrical field of the particle, they cannot orient with the external field, and the permittivity is low. Table 1 summarizes a few mixing models. It can be observed that the real permittivity of soils depends mainly on volumetric water content, clay content, porosity, saturation and frequency.

Table 1. Mixing models

Expression*	Notes	Reference
$\kappa'_m = [n(1-S)\sqrt{\kappa'_a} + nS\sqrt{\kappa'_w} + (1-n)\sqrt{\kappa'_s}]^2$	Complex refractive index model based on time of propagation for three-phase medium	Sen *et al.* (1981)
$\kappa'_m = \kappa'_s + \frac{f_w}{3}(\kappa'_w - \kappa'_s)\sum_{j=1}^{3} 1/\left[1 + \left(\frac{\kappa'_w}{\kappa'_{sw}} - 1\right)A_j\right]$	Assumes saturation and elliptical particles at microwave frequencies	DeLoor (1968) (see also van Beek, 1967)
$\kappa'_m = 40w_v - 3{\cdot}9 + \sqrt{(44{\cdot}8 - 392w_v + 1600{w_v}^2)}$	Frequency range between 1·0 and 1·50 GHz	Selig & Mansukhani (1975)
$\kappa'_{m_\infty} = 2{\cdot}5 + (0{\cdot}5 - w_v) + 4w_v$ $\kappa'_{m_s} = 3{\cdot}14 + 23{\cdot}83w_v + 91{\cdot}58{w_v}^2$ Apply within Debye's relaxation formula with selected relaxation frequency	Soil–water mixture at microwave frequencies	Wang (1980)
$W_p = 0{\cdot}06774 - 0{\cdot}00064S\% + 0{\cdot}00478C\%$ $W_t = 0{\cdot}49W_p + 0{\cdot}165$ $\kappa'_m = w_v\kappa'_x + (n - w_v)\kappa'_a + (1-n)\kappa'_s$ where $\kappa'_x = \kappa'_i + (\kappa'_w - \kappa'_i)\frac{w_v}{W_t}\gamma$ $\kappa'_m = W_t\kappa'_x + (w_v - W_t)\kappa'_w + (n - w_v)\kappa'_a + (1-n)\kappa'_s$ where $\kappa'_x = \kappa'_i + (\kappa'_w - \kappa'_i)\gamma$	Frequency ≈ 1·40 GHz For $w_v < W_p$ For $w_v > W_p$	Wang & Schmugge (1980)
$\left(\frac{\kappa'_m - \kappa'_s}{\kappa'_w - \kappa'_s}\right)\left(\frac{\kappa'_w}{\kappa'_m}\right)^{1/3} = n$	Saturated mixture at high frequencies	Sen *et al.* (1981)

* κ'_m, permittivity of mixture; κ'_s, permittivity of solids; κ'_w, permittivity of water; κ'_a, permittivity of air; κ'_i, permittivity of ice; κ'_{sw}, an intermediate value between κ'_s and κ'_w; w_v, volumetric water content; f_i, volume fraction of solids or water; n, porosity; S, saturation; A_j, depolarization factors; $S\%$, sand percentage; $C\%$, clay percentage; γ, adjustable parameter.

Mechanical waves—shear wave velocity

The frequency spectrum of velocity and attenuation characterizes the interaction between mechanical waves and materials. However, most research has focused on narrow-band velocity measurements. In the case of saturated soils, P-waves propagate through the solid phase as well as the liquid phase. However, S-waves propagate primarily through the solid matrix with minimum influence from the pore fluid. Thus, shear waves are preferred to study saturated soils.

The shear wave velocity V_s in a continuum is related to the shear stiffness $G(V_s) = \sqrt{(G/\rho)}$ where ρ is the mass density). In particulate media, the fabric, the contact forces and the contact laws acting (e.g. Hertz) determine the stiffness G of the medium. Empirical relations have been proposed to relate shear wave velocity to the state of stress in the polarization plane (Roesler, 1979):

$$V_s = \xi\left(\frac{\sigma'_x}{p_a}\right)^{\chi_x}\left(\frac{\sigma'_y}{p_a}\right)^{\chi_y} \tag{2}$$

where ξ, χ_x and χ_y are constants and σ'_x and σ'_y are the effective stresses in the direction of propagation and in the direction of polarization respectively. Stresses are normalized with respect to the atmospheric pressure p_a. Studies in our laboratory have shown that for some fabrics the correlation is also adequate in terms of the mean stress in the polarization plane, $\sigma'_{av} = (\sigma'_x + \sigma'_y)/2$ with minimum effect of the deviatoric component $\sigma'_d = (\sigma'_x - \sigma'_y)/2$:

$$V_s = \xi_a\left(\frac{\sigma'_{av}}{p_a}\right)^{\chi_{av}}\left(\frac{\sigma'_d}{p_a}\right)^{\chi_d} \approx \xi_a\left(\frac{\sigma'_{av}}{p_a}\right)^{\chi_{av}} \tag{3}$$

Thus, $\chi_d \approx 0$.

The shear stiffness of preloaded materials can be related to the current mean state of stress on the propagation plane σ'_{av} and the overconsolidation ratio R_0 defined in terms of the mean stress (see Houlsby & Wroth, 1991; Viggiani & Atkinson, 1995):

$$V_s = \xi_{av}\left(\frac{\sigma'_{av}}{p_a}\right)^{\chi_m} {R_0}^n \tag{4}$$

where n is a constant between 0·15 and 0·35. A similar modification ($R_0{}^n$) can be applied to equation (2). For normally consolidated soils under isotropic stresses, equations (2), (3), and (4) reduce to

$$V_s = \xi_{iso}\left(\frac{\sigma'_{iso}}{p_a}\right)^{\gamma} \tag{5}$$

where the exponent γ is equal to $\chi_m = \chi_x + \chi_y$ (γ is the slope of the log–log plot of velocity against effective stress). Micromechanical evidence for these relations has been presented elsewhere (Cascante & Santamarina, 1996; Santamarina & Cascante, 1996). The theoretical value for γ in the case of spherical particles follows from Hertz's theory and is equal to $\frac{1}{6}$. In the case of cone-to-plane contacts, $\gamma = \frac{1}{4}$ (Gladwell, 1980). Measurements of γ in real particulate materials show a variation from 0·17 to 0·48 (Aloufi & Santamarina, 1995; Thomann & Hryciw, 1990; Bates, 1989; Schultheiss, 1981).

Hamdi & Taylor (1981) and Shirley & Hampton (1978) monitored the increase in wave velocity during primary consolidation. They observed an increase in wave velocity with consolidation time. Anderson & Stokoe (1978) and Anderson & Woods (1976) measured the change in shear modulus G_{max} during primary and secondary consolidation using a resonant column device. G_{max} increased by up to 40% per log cycle of time during the secondary consolidation of soft Leda and Gulf of Mexico clays. The change in shear modulus could not be explained by changes in void ratio using existing empirical equations (e.g. Hardin & Richart, 1963).

EXPERIMENTAL STUDY

The experimental study reported in this paper was designed to assess information at the micro-level during consolidation, by means of electromagnetic and mechanical waves.

Device and instrumentation

A special oedometer cell was designed and built to introduce a pore pressure transducer, piezoelectric bender elements for sending and receiving shear waves and a probe for measuring dielectric permittivity. Details of the cell design are presented in Fam & Santamarina (1995). A porous stone was connected to the upper plate to provide drainage. The base of the cell has three orifices to house the instrumentation. The upper plate has a slot for the matching piezocrystal element. A schematic diagram of the oedometric cell and the instrumentation are shown in Fig. 1.

Dielectric permittivity was measured with a coaxial terminator probe (HP 85070A) integrated with a network analyser (HP 8752A). Shear wave velocity through the sample was monitored using piezocrystal bender elements (PZT-5, APC). The pore pressure transducer was connected to the base through a small-diameter tube that was covered by a larger porous plate supported on the base. This design eliminates the transmission of fabric stresses.

All measurements can be characterized as either local parameters or average–global parameters. The pore pressure transducer and the dielectric coaxial terminator locally assess the specimen in their vicinity. Therefore, pore water pressure and permittivity are local parameters. On the other hand, shear wave velocity and settlement are measured across the sample height, therefore they are average–global parameters. Relationships were evaluated among local or global parameters, but not combined, unless integration of local into global or inversion of global to local could be performed.

Tested materials—sample preparation

Three soils were tested in this experimental programme: silica flour, kaolinite and bentonite. They were chosen to have a wide range of inter-particle forces: physical contacts, short-range forces and long-range forces (Mitchell, 1993). The physical, chemical and engineering properties of the

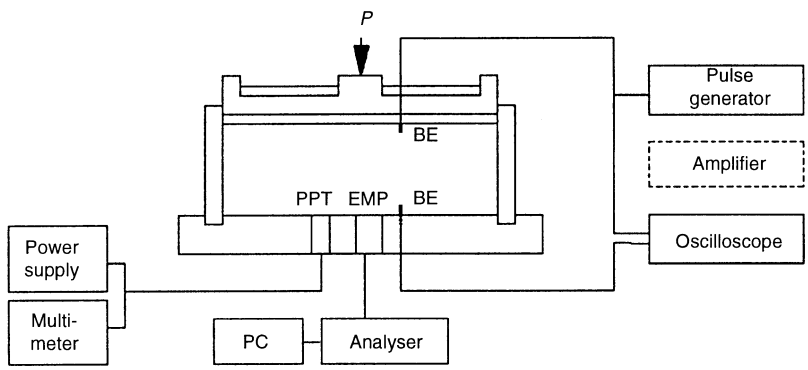

Fig. 1. Schematic diagram of oedometric cell and main measuring devices: BE, bender element; EMP, electromagnetic probe; PPT, pore pressure transducer

tested materials are summarized in Table 2. Samples were prepared using the slurry consolidation techniques (Sheeran & Krizek, 1971). Dry soil was placed in a mixer and distilled water was added continuously while mixing until the water content was twice the liquid limit w_l ($w \approx 2w_l$). During mixing, vacuum was applied to the container to remove air pockets. The sample was left in a closed container for 24 h to ensure saturation, hydration and homogeneity. The slurry was poured into a split mould with an internal rubber membrane. The set was left to consolidate under 50 kPa. After consolidation, the mould was removed, the specimen was checked and a sample was taken from the clay to measure the final water content.

RESULTS AND ANALYSES

The results presented and discussed in this paper centre on the study of kaolinite. Whenever appropriate, data for silica flour and bentonite are presented to highlight similarities and differences. Additional consolidation data was obtained for bentonite in an isotropic cell where double drainage was permitted (a one-load increment test was run in the modified oedometer, from a virtual contact load to 100 kPa.)

Standard geomechanical parameters

The $e-\log(\sigma'_x)$ plot for kaolinite is shown in Fig. 2(a), during loading, unloading and reloading cycles. Computed consolidation parameters for the tested soils are summarized in Table 2.

The void ratio at the base of the sample e_l (local) was computed from the measured volume changes (global) and excess pore water u_l (local), assuming Terzaghi's linear relationship between void ratio and pore pressure

$$e_l = e_f + (e_0 - e_f)\left(\frac{u_l}{u_0}\right) \tag{6}$$

where e_0 is the initial void ratio before loading, e_f is the final void ratio after consolidation and u_0 is the initial pore water pressure measured immediately after loading. Fig. 2(b) presents a typical change in average and local void ratios with time for one load cycle in kaolinite (from 305 kPa to 610 kPa). Note that the measured average void ratio continues decreasing during secondary consolidation.

Dielectric permittivity

Dielectric permittivity measurements were recorded with time during each load increment. Table 3 summarizes the range of measured permittivity values for the three soils. Typical spectral plots for the complex permittivity are shown in Fig. 3. A significant increase in real permittivity is observed with decrease in frequency for bentonite. The imaginary component for bentonite continuously decreases with increasing frequency, unlike silica flour and kaolinite. This difference in behaviour highlights the higher influence of double-layer polarization and low-frequency losses in bentonite compared with kaolinite and silica flour. Double-layer relaxation in bentonite masks the beginning of free-water polarization, which is seen in kaolinite and silica flour (this is reflected in the increase in the imaginary permittivity κ'' starting at frequencies $>$ 0·50 GHz).

The change in the complex permittivity of kaolinite with frequency and stress level is shown in Fig. 4 at the end of each consolidation level. A similar graph was observed for silica flour but with smaller values. Fig. 5 summarizes the evolution of the complex permittivity of 0·2 GHz and 1·3 GHz,

Table 2. Properties of tested soils and loading range

Soil type	Silica flour	Kaolinite	Bentonite
Source	Indusmin Co., Toronto, Canada	Vanderbilt Co., Los Angeles, USA	Saskatchewan, Canada
Trade name	Silex Regular	Peerless clay	Avonseal or Geoseal
Colour	White	Light cream	Light tan
Specific gravity	2·65	2·6	2·55
Liquid limit	—	50	250
Plastic limit	—	35	50
CEC	—	20–30	80–85
pH value	7·0 (10% solids)	4·8 (10% solids)	9·0 (5% solids)
Loading range			
Vertical stress: kPa	0–610	0–610	0–100 (Oed.) 0–480 (Iso.)
Void ratio e	0·78–0·69	1·57–0·94	8·9–4·61 (Oed.) 5·71–3·0 (Iso.)
Compression coefficient C_c	0·06	0·46	3·30

Oed., oedometer; Iso., isotropic.

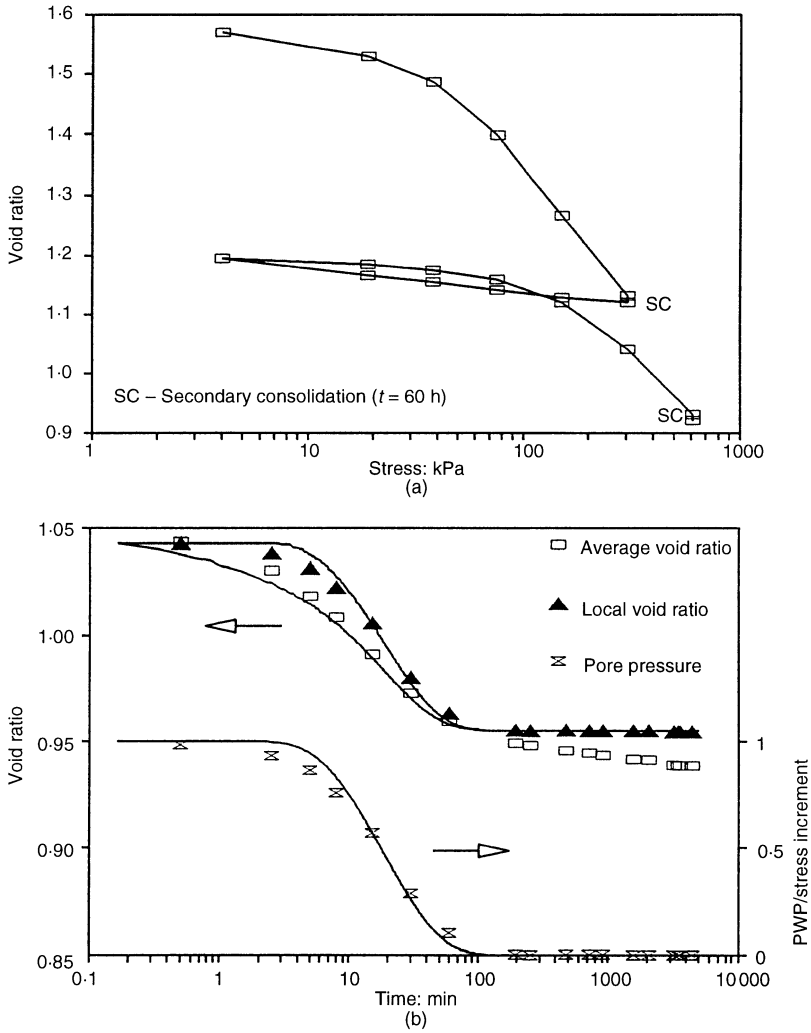

Fig. 2. Kaolinite sample: (a) e–log$p$ curve; (b) measured average e and estimated local e at the base of the sample ($\sigma = 305$–610 kPa, note that trend reflects the single drainage condition)

Table 3. Summary of measured complex permittivity values for the three tested soils

		Soil					
Parameter		Silica flour		Kaolinite		Bentonite	
Water content: %		29	26	60	36	349	180
Real permittivity	0·20 GHz	23·8	21·6	35·6	27·7	77·4	75·5
	1·30 GHz	23·4	21·3	35·0	27·1	55·7	50·1
Imaginary permittivity*	0·20 GHz	2·0	1·7	2·5	2·1	128	125
	1·30 GHz	1·8	1·5	2·3	1·7	16·6	15·9

* Silica flour and kaolinite show minima at intermediate frequencies, see Fig. 3(b).

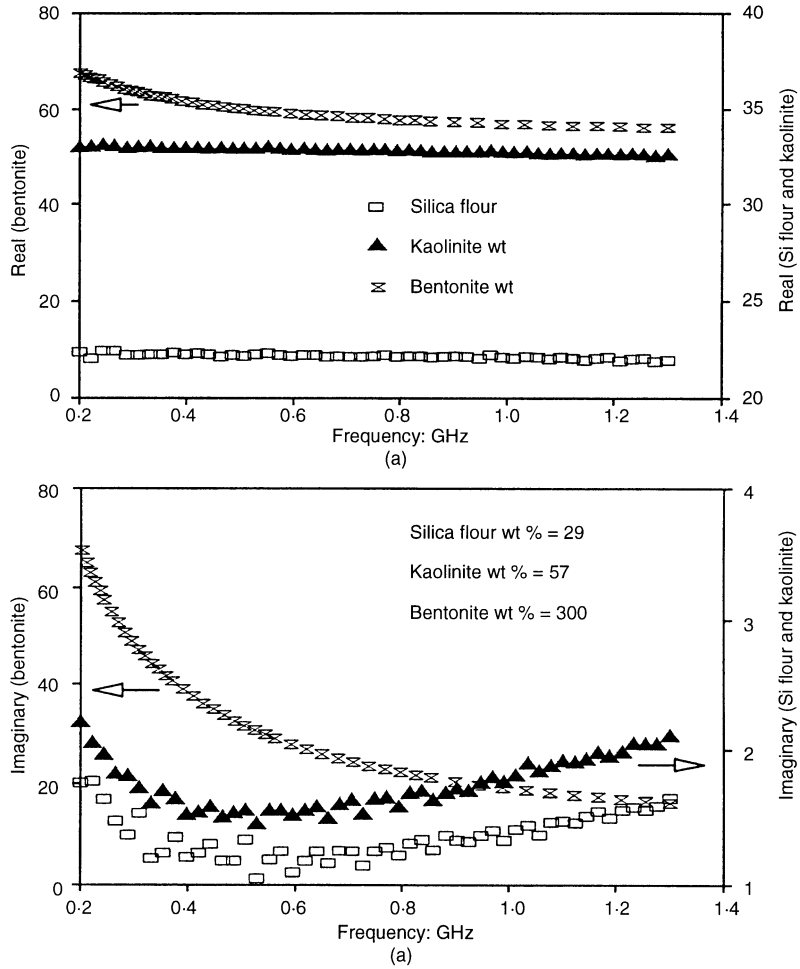

Fig. 3. Typical change in the complex permittivity with frequency for silica flour, kaolinite and bentonite: (a) real; (b) imaginary

plotted against the volumetric local water content for the complete loading history (see equations (1) and (6)).

The spectral response for the real permittivity shifts down with the increase in the stress level. This shift reflects the overall decrease in water content. Since spectral responses are parallel for the different stress levels (Fig. 4(a)), it appears that consolidation affects mainly free water (polarizability accumulates from high to low frequencies). The trends in imaginary permittivity confirm this observation. At low frequencies, the real permittivity κ' converges to the same value regardless of the stress level (Fig. 4(b)) (it remains constant in Fig. 5(b)). However, losses at 1·30 GHz show a clear reduction with higher loads, indicating a reduction in free water (Fig. 5(b)).

These trends in polarizability and losses indicate that the consolidation of kaolinite in this load range may not be explained by the modified effective stress σ_m based on long-range forces between parallel plates (Sridharan & Jayadeva, 1982):

$$\sigma_m = \sigma_t - u - (R_{DL} - Att) \tag{7}$$

where u is the average pore water pressure, σ_t is the total stress, R_{DL} is the double-layer repulsion and Att is the van der Waals attraction. These results agree with observations by Santamarina & Fam (1995), who showed that shear wave velocity changes in kaolinite due to concentration diffusion reflected a prevailing effect of short-range forces. The lack of data for bentonite in the full con-

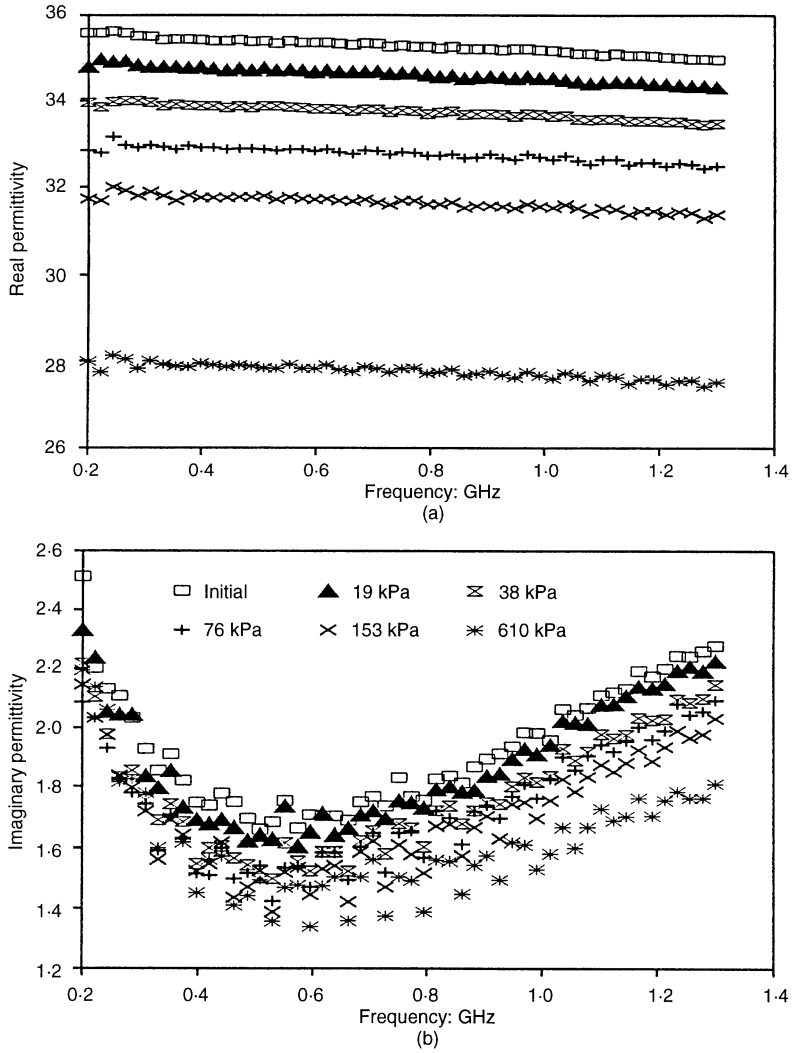

Fig. 4. Spectral response at the end of consolidation for kaolinite sample: (a) real; (b) imaginary

solidation range does not permit extending this discussion to colloidal, lattice-expanding clay minerals.

An approximately linear relationship between the real permittivity κ' and the volumetric water content w_{vol} is observed in Fig. 5(a). A parallel study conducted with different specimen preparation techniques showed similar results, demonstrating that the fabric has almost no effect on permittivity at microwave frequencies.

Mixture models listed in Table 1 are superimposed on Fig. 5(a). Unknown parameters were selected on the bases of known ranges and optimized by fitting equations to the data. Best results were obtained with the model of DeLoor; the permittivity of bound water was assumed equal to the permittivity of solid particles ($\kappa'_{sw} = \kappa'_{s} = 3$), and disc-shaped particles were considered ($A_j = 1$, 0, 0). Empirical models show significant deviations.

The changes in volumetric water content during the two secondary consolidation cycles imposed on the kaolinite were too small to affect the high-frequency permittivity. On the other hand, relative displacements at the level of the double layer do not necessarily imply changes in polarization at low frequency.

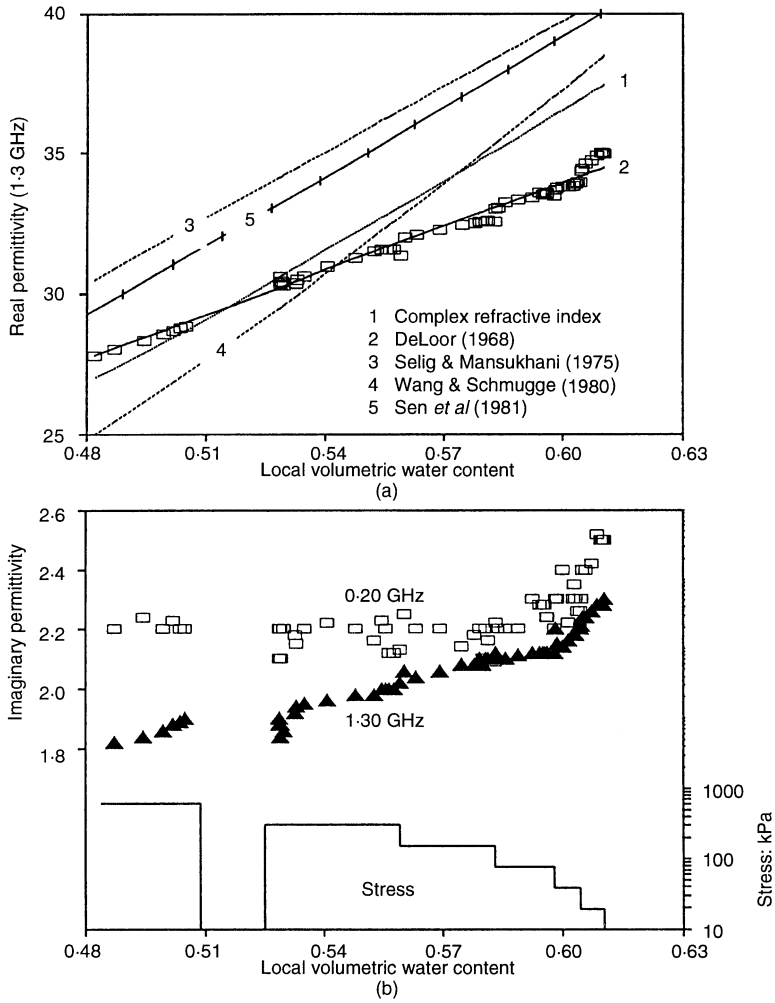

Fig. 5. Complex permittivity during the consolidation of kaolinite plotted against local volumetric water content at 0·20 and 1·30 GHz: (a) real—1·30 GHz and mixing models; (b) imaginary

Shear wave velocity

Shear wave velocity is an average–global measurement. It was calculated by dividing the distance travelled, H, by the travel time t. The distance H is the momentary height of the sample corrected for bender element penetration inside the sample. Shear wave velocity is plotted against time in Fig. 6. The increase in shear wave velocity during primary consolidation reflects the dissipation of pore pressure and the ensuing increase in skeletal forces which cause fabric changes (contact gain or loss and particle reorientation).

The shear wave velocity at the end of each load increment is plotted against the vertical effective stress in Fig. 7. The scales are presented in log–log form to highlight the nature of the power relation. Points along virgin loading fit a straight line; however, the velocity is higher during unloading. These residual effects reflect not only the higher state of horizontal stress when the over-consolidation ratio $R_0 > 1$, but also permanent fabric changes.

Barbour & Fredlund (1989) showed that the relationship between ($R_{DL} - Att$) and the vertical stress is non-linear, so that an increase in the applied pressure will not only increase the electrical ($R_{DL} - Att$) stress but also increase contact stresses (or short-range forces). A model based on non-parallel plates with face-to-edge contacts can manifest such behaviour (e.g. Bolt, 1956; Hueckel,

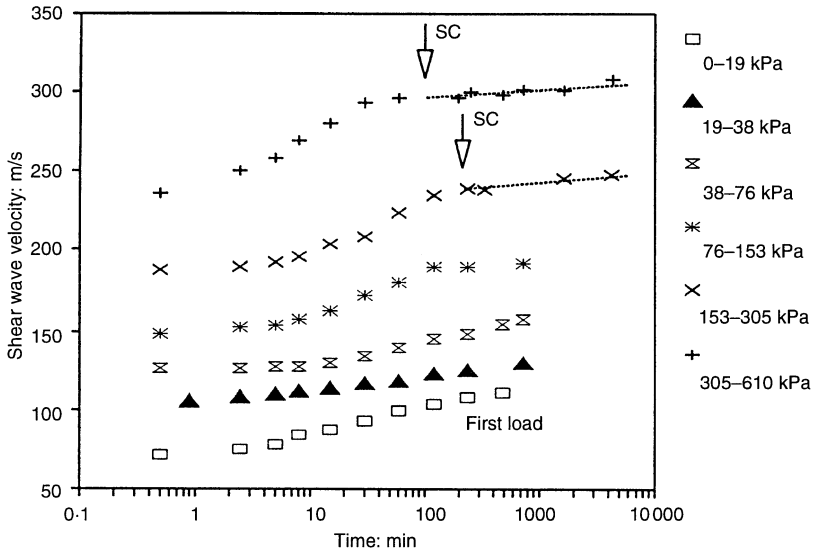

Fig. 6. Shear wave velocity during consolidation of kaolinite under different stress levels

1992). The change in small-strain shear stiffness during the consolidation of kaolinite is in agreement with these observations.

Altogether, permittivity and shear wave velocity data indicate that the consolidation of kaolinite, in the stress range studied, increases contact forces and reduces the volume of free water, without altering the level of double-layer phenomena.

The change in shear wave velocity during secondary consolidation is shown in Fig. 6. In agreement with Anderson & Stokoe (1978), the increase in velocity is linear with the logarithm of time. The soil evolves towards a lower energy level during secondary consolidation, gaining small-strain stiffness in the process (see also Anderson & Woods, 1976).

Initial drop of shear wave velocity

Figure 8(a) shows the change in shear wave velocity during early stages of consolidation for the three soils. Two salient observations can be made: (1) the delay in the increase in velocity is higher for soils with lower permeability, and (2) there is a drop in shear wave velocity just after loading kaolinite and bentonite samples. Changes in silica flour occurred too fast to measure the transient stage. The average decrease in velocity was about 5%.

Hardin & Black (1968) and Schultheiss (1981) also noticed a drop in shear wave velocity immediately after loading. Hardin & Black (1968) presumed that a sudden breakdown in microstructure had occurred. Schultheiss (1981) speculated that the excess pore pressure near transducers altered the drainage path and affected the measured velocity. Afifi & Woods (1971) measured a significant drop in velocity after loading dry kaolinite.

Altered drainage paths would not cause a measurable effect, given the geometry of the cell used in this study. Yet, another measurement effect could be present: the induced pore pressure produces the elastic expansion of the shell, leading to the relaxation of the effective horizontal stresses, and to the reduction in shear wave velocity according to equation (2). This hypothesis was tested by comparing Plexiglas and stainless steel cells using bentonite specimens. A similar velocity drop was measured in both cases. Furthermore, computations based on ring formulae and equation (2) showed that stress relaxation could only explain a velocity drop lower than 0·6%.

The hypothesis based on the sudden breakdown in microstructure or 'de-structuration' requires immediate deformation in the soil–water mixture on loading, and a pore pressure parameter $C < 1{\cdot}0$. Furthermore, it would imply that the new fabric has a lower small-strain stiffness. Ongoing studies in our laboratories with visco-plastic materials such as lead shot and granular salt show that attenuation increases immediately on loading, returning to lower levels with time; however, we have observed no transient in velocity (Cascante & Santamarina, 1996). Higher attenuation may lead to the apparent

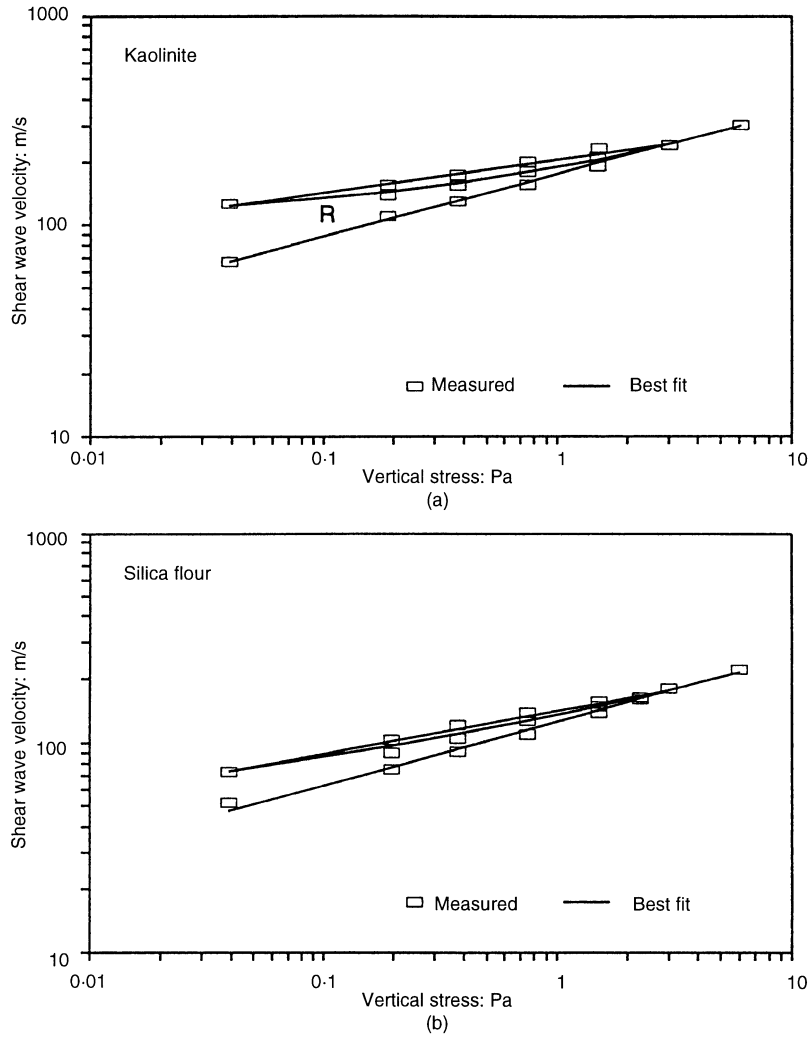

Fig. 7. Shear wave velocity at the end of primary consolidation plotted against vertical stress during loading, unloading and reloading: (a) kaolinite; (b) silica flour; best-fit line corresponds to equation (2) modified for preloading; L, load; U, unload; R, reload

increase in travel time owing to the more difficult detection of first arrivals. This would be particularly misleading if automated travel time measuring systems based on threshold amplitude are used. All results reported in this study were obtained by hand-picking first arrivals. Other possible effects near the transducers are not likely to contribute to the travel time integral across the specimen.

An alternative hypothesis is the uneven distribution of pore pressure in the sample, resulting in non-uniform effective stress distribution immediately on loading. Such a condition could develop because of the multi-dimensional consolidation behaviour within the specimen (Mandel–Cryer effect: Cryer, 1963; Lee *et al.*, 1983; Chopra & Dargush, 1995). However, measured pore pressures (e.g. Fig. 2(b)) do not support this hypothesis. Spatial differences in stiffness could also cause a non-uniform pore pressure distribution, due, for example, to the presence of 'granularities' within the soil mass. Recalling that the relationship between shear velocity and effective stress is non-linear (equations (2)–(4) and Fig. 8(b)), the integral travel time across the sample results in a velocity 5% smaller than V_{mean}, for a coefficient of variation in effective stress $COV = 40\%$ ($COV =$

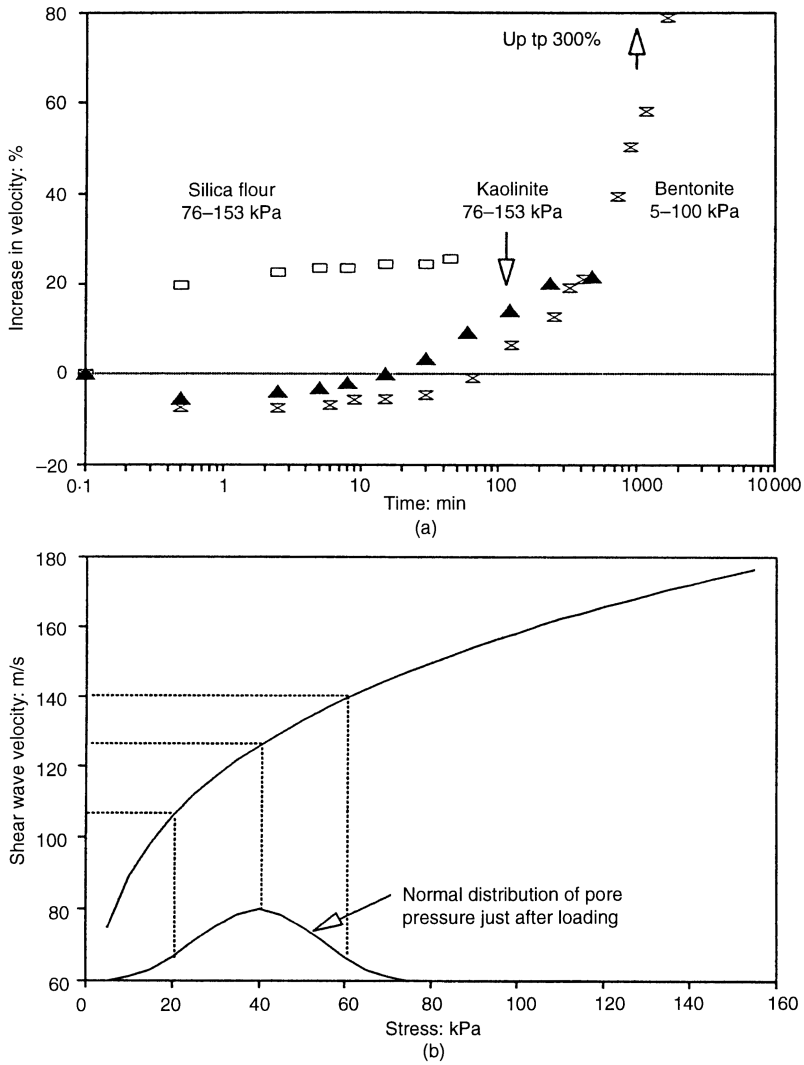

Fig. 8. (a) Evolution of shear wave velocity with time for silica flour, kaolinite and bentonite; (b) effect of pore pressure distribution on measured shear wave velocity immediately after loading

standard deviation/mean). If the uneven pore pressure hypothesis is correct, the time required for the shear wave velocity to return to its initial value may indicate the average local permeability of the soil. Bentonite showed a longer 'recovery' time than kaolinite, which is consistent with the lower permeability of bentonite.

Shear wave velocity–stress relationships

The data presented in Fig. 7 can be used to determine the constants in equations (2) and (4). However, stress changes and fabric changes affect these parameters; hence, the analysis must differentiate between loading, unloading and reloading regimes, as proposed in equation (4).

The horizontal stress was estimated using the empirical relationship for the coefficient of horizontal earth pressure at rest, K_0, proposed by Mayne & Kulhawy (1982). The least square error method was used to find the best-fit model of the data. The results are plotted in Figs 7 and 9 as continuous lines, and the corresponding inverted parameters are shown in Table 4. Note that the data in Fig. 9 are normalized by the correction factor for preloading.

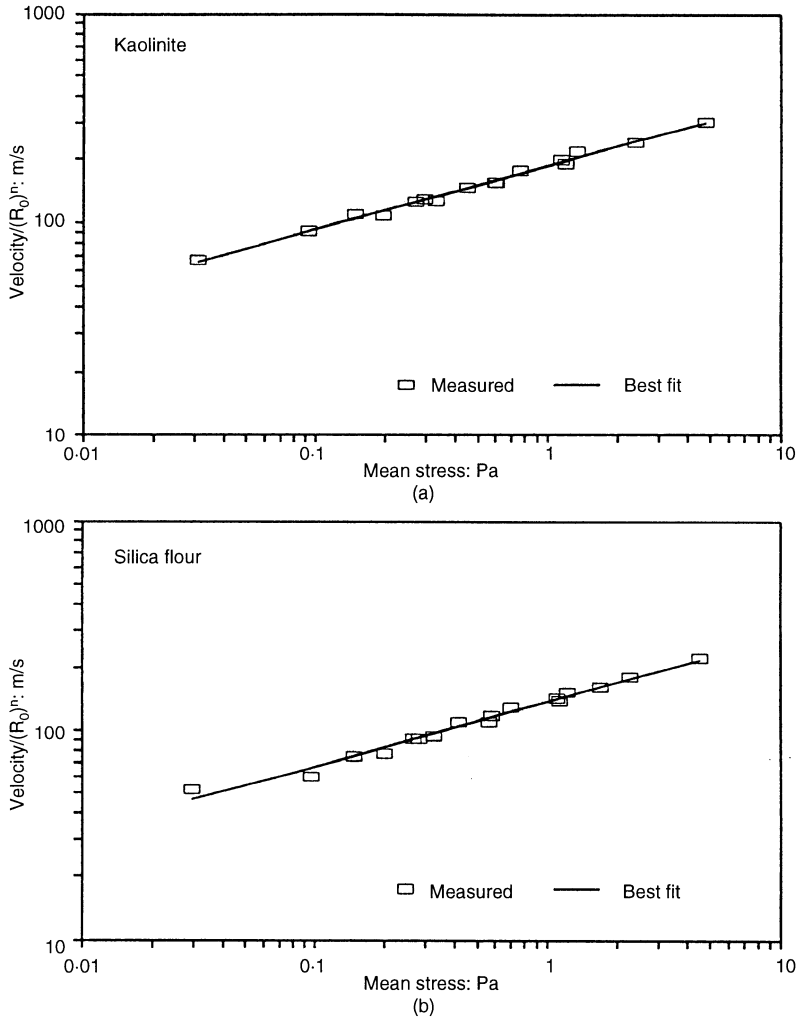

Fig. 9. Measured shear wave velocity at the end of primary consolidation plotted against mean stress in the polarization plane during loading, unloading and reloading: (a) kaolinite; (b) silica flour; best-fit line corresponds to equation (4)

While the average square error per measurement is slightly different, both models adequately match the variation of shear wave velocity. The variation of computed exponents as a function of ϕ is very small (see range of exponents for a $\pm 5°$ range in ϕ values used in the equation for K_0 in Table 4). In kaolinite, the exponent for the stress in the transverse direction is greater than the exponent for the longitudinal stress. This is not the case for silica flour.

The exponent n for the overconsolidation ratio R_0 was higher in kaolinite than in silica flour ($n = 0{\cdot}10$ in kaolinite and $n = 0{\cdot}06$ in silica flour). The same velocity–stress model was applied to similar data obtained with a sand specimen, resulting in $n = 0$. Note that the computation of velocity with either of the velocity–stress models takes into consideration the higher horizontal stresses locked in during preloading. Thus, the ${R_0}^n$ coefficient can be interpreted as a correction factor for fabric changes during loading and unloading. Indeed, the plot of ${R_0}^n$ is in close agreement with other empirical formulae that correct for changes in void ratio (e.g., Hardin & Ritchart, 1963). Therefore, the exponent n should increase with the increase in soil plasticity. This is consistent with results obtained by Viggiani & Atkinson (1995).

The change in shear wave velocity in bentonite due to an increase in effective stress was obtained

Table 4. Velocity–stress relations*

	Model			
	Longitudinal and transverse stress (equation (2) modified)		Mean stress in polarization plane (equation (4))	
Soil	Constants	Average error: m/s	Constants	Average error: m/s
Kaolinite ($\phi = 25° \pm 5°$)	$\xi = 195 \pm 5{\cdot}6$ $\chi_x = 0{\cdot}097 \pm 0{\cdot}01$ $\chi_y = 0{\cdot}20 \pm 0{\cdot}01$ $n = 0{\cdot}08 \pm 0{\cdot}015$	$5{\cdot}27 \pm 0{\cdot}11$	$\xi = 187 \pm 3$ $\chi_{av} = 0.301 \pm 0.002$ $n = 0{\cdot}10 \pm 0{\cdot}005$	$5{\cdot}24 \pm 0{\cdot}07$
Silica flour ($\phi = 30° \pm 5°$)	$\xi = 138 \pm 2{\cdot}2$ $\chi_x = 0{\cdot}168 \pm 0{\cdot}007$ $\chi_y = 0{\cdot}137 \pm 0{\cdot}013$ $n = 0{\cdot}06 \pm 0{\cdot}008$	$4{\cdot}43 \pm 0{\cdot}15$	$\xi = 136 \pm 1{\cdot}5$ $\chi_{av} = 0{\cdot}309 \pm 0{\cdot}001$ $n = 0{\cdot}06 \pm 0{\cdot}008$	$3{\cdot}97 \pm 0{\cdot}21$

* The range of each parameter was calculated for a $\pm 5°$ range in the angle of shearing resistance. Inverted parameters are little sensitive to the value of ϕ used in the K_0 equations.

from isotropic load tests with efficient drainage conditions. The computed exponent γ was 0·443 (see also Schultheiss, 1981). Viggiani & Atkinson (1995) concluded that the power coefficient γ increases with the plasticity index *PI* of the clay (the coefficient ξ_{iso} decreased with *PI*).

Comparing the exponents obtained for bentonite, kaolinite and silica flour, it can be concluded that the velocity–stress relationship depends on

(*a*) the ability to change the microstructure (larger γ with larger changes—see also Hryciw & Thomann, 1993; Endres, 1990; Aloufi & Santamarina, 1995)
(*b*) the significance of interparticle electrostatic forces (see also Santamarina & Fam, 1995)
(*c*) the nature of the mechanical contact law (e.g. Hertzian—see Cascante & Santamarina, 1996).

Silica flour is governed mainly by microstructural changes and contact behaviour. Bentonite is controlled by the first two mechanisms. Finally, kaolinite is influenced by all three mechanisms.

FIELD APPLICATION: TOMOGRAPHIC MONITORING

Results presented in this paper show that changes during the consolidation of soils cause changes in the propagation parameters of mechanical and electromagnetic waves. These observations could lead to a variety of non-invasive techniques to monitor in situ the consolidation of geosystems using waves, either ground penetrating radar (GPR) data (changes in water content) or seismic data (changes in effective stress). If data are gathered in multiple directions, 'projections' can be processed with standard inversion techniques to produce a tomogram. The potential of seismic wave tomography to monitor stress changes in dry soils has already been shown (Santamarina & Potts, 1994). The same concept can be generalized to invert and to monitor the spatial distribution of effective stress (equation (2)) and pore pressure during consolidation in the field.

Measured travel times t are the integral of local velocities $V(x, y)$ along the ray path l, from the source s to the receiver r:

$$t = \int_s^r \frac{\mathrm{d}l}{V(x, y)} \quad \text{(for each ray)} \tag{8}$$

If the medium is discretized in pixels, equation (8) can be expressed in matrix form:

$$\boldsymbol{t} = L\boldsymbol{s} \tag{9}$$

where $\boldsymbol{t}$ is the vector of measured travel times, L is the matrix of lengths travelled by each ray in each pixel and is computed by geometry, and $\boldsymbol{s}$ is the vector of unknown pixel slowness, $s = 1/V$. Usually L is not invertible. A robust alternative method of solving for $\boldsymbol{s}$ is regularization,

$$\boldsymbol{s} = (L^{\mathrm{T}}L + \lambda R^{\mathrm{T}}R)^{-1}\boldsymbol{t} \tag{10}$$

where λ is a constant to be optimized and R is the regularization matrix (Santamarina & Gheshlaghi, 1995). The matrix R must be selected to satisfy the physics of the phenomenon being monitored. In the case of consolidation, water content and effective stress are related to pore pressure. The space–time distribution of pore pressure is governed by Terzaghi's equation, which can be used as a regularization function for tomographic process monitoring. Likewise, the spatial distribution of the real and imaginary permittivity can be inverted from GPR data, and converted to the spatial distribution of water content using relationships such as those shown in Fig. 5(a). Knowing the distribution of water content, the average degree of consolidation can be determined.

SUMMARY AND CONCLUSIONS

Complementary measurements with mechanical and electromagnetic waves have been successfully implemented during the consolidation of three soils of different physico-chemical properties. The salient observations are as follows:

(*a*) Changes in the high-frequency complex dielectric permittivity during the consolidation of kaolinite indicate a decrease in free water inside the sample. There is no indication of changes in double-layer polarizability for effective confining stresses less than 610 kPa. The combined analysis of changes in the polarizability κ' and losses κ'' facilitates the interpretation of spectral measurements.

(*b*) The polarization of double layers masks the beginning of the relaxation polarization of the free water (≈0·5 GHz) in the case of materials with significant double-layer phenomena such as bentonite. Changes in the real permittivity at microwave frequencies with soil water content can be approximated by a linear relationship if the decrease in volume is only due to the reduction in free water. At high frequencies, permittivity is not sensitive to fabric.

(*c*) The velocity of propagation of shear waves clearly reflects the transfer of load from pore pressure to skeletal stresses, and the corresponding increase in stiffness during primary and secondary consolidation. Velocity–stress relationships can be used to assess the contribution of mechanical and electrostatic interparticle forces, contact behaviour and changes in microfabric.

(*d*) Permittivity and shear wave velocity data indicate that the consolidation of kaolinite in the stress range studied increases contact forces and reduces the volume of free water, without altering the level of double-layer phenomena.

(*e*) The shear wave velocity (and hence the small-strain shear stiffness) drops immediately after loading. It is hypothesized that this observation indicates non-uniform pore pressure response inside the sample. Indeed, the time required to recover the initial stiffness, which is the time needed for the homogenization of pore pressure, depends on soil permeability.

(*f*) Shear wave velocity is influenced by effective stresses in the directions of propagation and polarization and by the overconsolidation ratio. The relative contribution of the stresses in the longitudinal and transverse directions cannot be inferred from K_0 virgin loading; however, it can be determined during unload and reload cycles. In the kaolinite tested, the exponent of the transverse stress is higher than the exponent of the longitudinal stress.

(*g*) The significance of the observed changes supports the potential development of field monitoring techniques, such as tomographic monitoring of consolidation processes underneath foundations and other geosystems, using mechanical and/or electromagnetic waves. Regularization functions can be selected to capture adequately the physics of the process.

ACKNOWLEDGEMENTS

This study was conducted by the authors during their affiliation with the Department of Civil Engineering, University of Waterloo. Funding was provided by the Natural Sciences and Engineering Research Council of Canada (NSERC). The authors are thankful to Professor E. Matyas (University of Waterloo) for multiple suggestions. The reviewers made valuable recommendations.

NOTATION

Att	attractive stress between clay particles
e	void ratio
e_0, e_f, e_l	initial, final, and local void ratios
G	shear modulus
H	sample height
h_t	total head
K_0	coefficient of lateral earth pressure
L	matrix of travel lengths
n	exponent for preloading correction
p_a	atmospheric pressure
R	regularization matrix
R_0	overconsolidation ratio
R_{DL}	repulsive stress between clay particles
s	slowness ($s = 1/V_s$)
t	travel time
u	pore water pressure
u_0, u_f, u_l	initial, final and local pore water pressures
V_s	shear wave velocity
w_l	liquid limit
w_{vol}	volumetric water content
γ, ξ, χ	constants for the velocity–stress power equation
κ'	relative real permittivity
κ''	relative imaginary permittivity
ρ	mass density
σ'_{av}	mean stress in plane of shear wave polarization $(\sigma'_x + \sigma'_y)/2$
σ'_{iso}	isotropic stress
σ_m	modified effective stress
σ_t	total stress
σ'_x	longitudinal stress
σ'_y	transverse stress
ϕ	angle of shearing resistance

REFERENCES

Afifi, S. S., & Woods, R. D. (1971). Long term pressure effects on shear modulus of soils. *J. Soil Mech. Fdns, ASCE* **97**, SM10, 1445–1460.

Aloufi, M. & Santamarina, J. C. (1995). Low and high strain macrobehavior of grain masses—the effect of

particle eccentricity. *Trans. ASAE* **38**, No. 3, 877–887.

Anderson, G. G. & Stokoe, K. H. (1978). Shear modulus: a time-dependent soil property. In *Dynamic Geotechnical Testing*, ASTM STP 654, pp. 66–90. American Society for Testing and Materials.

Anderson, G. D. & Woods, R. D. (1976). Time-dependent increase in shear modulus of clay. *J. Geotech. Engng, ASCE* **102**, GT5, 525–537.

Barbour, S. L. & Fredlund, D. G. (1989). Mechanisms of osmotic flow and volume change in clay soils. *Can. Geotech. J.* **26**, 551–562.

Bates, C. R. (1989). Dynamic soil property measurements during triaxial testing. *Géotechnique* **39**, No. 4, 721–726.

Bolt, G. H. (1956). Physico-chemical analysis of the compressibility of pure clays. *Géotechnique* **6**, No. 2, 86–93.

Cascante, G. & Santamarina, J. C. (1996). Interparticle contact behaviour and wave propagation. *ASCE Geotech. J.* **122**, No. 10, 831–839.

Chopra, M. B. & Dargush, G. F. (1995). Boundary element analysis of stresses in an axisymmetric soil mass undergoing consolidation. *Int. J. Numer. Anal. Methods Geomech.* **19**, 195–218.

Cryer, C. W. (1963). A comparison of the three-dimensional consolidation theories of Biot and Terzaghi. *Quart. J. Mech. Applied Math*. **XVI**, 401–411.

Debye, P. (1929). *Polar molecules*. New York: Chemical Catalog Company.

DeLoor, G. P. (1968). Dielectric properties of heterogeneous mixtures containing water. *J. Microwave Power* **3-2**, 67–73.

Dobson, M. C. & Ulaby, F. T. (1981). Microwave backscatter dependence on surface roughness, soil moisture, and soil texture—part III: soil tension. *IEEE Trans. Geosci. Remote Sensing* **GE-19**, 51–61.

Dukhin, S. S. & Shilov, V. N. (1973). Dielectric phenomena and the double layer in disperse systems and polyelectrolytes. Translated from Russian by D. Lederman. New York: Wiley.

Endres, A. L. (1990). The effect of contact generation on the elastic properties of granular medium. *J. Appl. Mech.* **57**, 330–366.

Fam, M. & Santamarina, J. C. (1995). Study of geoprocesses with complementary wave measurements in an oedometer. *ASTM Geotech. Testing J.* **18**, No. 3, 307–314.

Fam, M. & Santamarina, J. C. (1996). Coupled diffusion–fabric-flow phenomena: an effective stress analysis. *Can. Geotech. J.* **33**, No. 3, 515–522.

Gladwell, G. M. L. (1980). *Contact problems in the classical theory of elasticity*. Germantown, MD: Sijthoff & Noordhoff.

Hamdi, F. A. & Taylor, S. D. (1981). Soil consolidation behavior assessed by seismic velocity measurements. *Geophys. Prospect.* **29**, 715–729.

Hardin, B. O. & Black, W. L. (1968). Vibration modulus of normally consolidated clay. *J. Soil Mech. Fdns., ASCE* **94**, SM2, 353–369.

Hardin, B. O. & Richart, F. E. (1963). Elastic wave velocities in granular soils. *J. Soil Mech. Fdns, ASCE* **89**, SM1, 33–65.

Hasted, J. B. (1973). *Aqueous dielectrics*. London: Chapman and Hall.

Hill, N. E., Vaughan, W. E. & Davis, M. (1969). *Dielectric properties and molecular behavior*. London: Van Nostrand Reinhold.

Houlsby, G. T. & Wroth, C. P. (1991). The variation of shear modulus of clay with pressure and overconsolidation ratio. *Soils Fdns* **31**, No. 3, 138–143.

Hryciw, R. D. & Thomann, T. G. (1993). A stress-history-based model for G^e of cohesionless soils. *J. Geotech. Engng, ASCE* **119**, No. 7, 1073.

Hueckel, T. A. (1992). On the effective stress concepts and deformation in clays subjected to environmental loads: Discussion. *Can. Geotech. J.* **29**, 1120–1125.

Jonscher, A. K. (1983). *Dielectric relaxation in solids*. London: Chelsea Dielectric Press.

Lee, I. K., Ingles, O. G. & White, W. (1983). *Geotechnical engineering*. Pitman. Massachusetts.

Lyklema, J., Dukhin, S. S. & Shilov, V. N. (1983). The relaxation of the double layer around colloidal particles and the low-frequency dielectric dispersion. *J. Electroanal. Chem.* **143**, 1–20.

Mayne, P. & Kulhawy, F. (1982). Ko-OCR relationship in soil. *J. Geotech. Engng, ASCE* **108**, GT6, 851–872.

Mitchell, J. K. (1993). *Fundamentals of soil behavior*, 2nd edn. New York: Wiley.

Okonski, C. T. (1960). Electric properties of macromolecules. V. Theory of ionic polarization in polyelectrolytes. *J. Phys. Chem.* **64**, 605–618.

Olsen, R. E. & Ladd, C. C. (1979). One dimensional consolidation problems. *J. Geotech. Engng, ASCE* **105**, GT1, 11–30.

Roesler, S. K. (1979). Anisotropic shear modulus due to stress anisotropy. *J. Geotech. Engng, ASCE* **105**, GT7, 871–880.

Santamarina, J. C. & Cascante, G. (1996). Stress anisotropy and wave propagation—a micromechanical view. *Can. Geotech. J.* **33**, No. 5, 770–782.

Santamarina, J. C. & Fam, M. (1995). Changes in dielectric permittivity and shear wave velocity during concentration diffusion. *Can. Geotech. J.* **32**, No. 4, 647–659.

Santamarina, J. C. & Fam, M. (1997). Dielectric permittivity of soils mixed with organic and inorganic fluids (0.02 GHz to 1.30 GHz). *J. Environ. Engng Geophys.*, March.

Santamarina, J. C. & Gheshlaghi, F. (1995). Tomographic imaging: potentials and limitations. *Proc. SPIE Conf. on Non-destructive Evaluation of Aging Structures and Dams, SPIE 2457, Oakland, California*, pp. 67–78.

Santamarina, J. C. & Potts, B. D. (1994). On the imaging of stress changes in particulate media: an experimental study. *Can. Geotech. J.* **31**, No. 2, 215–222.

Schultheiss, P. J. (1981). Simultaneous measurements of P & S wave velocities during conventional laboratory soil testing procedures. *Marine Geotechnol.* **4**, No. 4, 343–367.

Schurr, J. M. (1964). On the theory of the dielectric dispersion of spherical colloidal particles in electrolyte solution. *J. Phys. Chem.* **68**, 2407–2413.

Schwarz, G. (1962). A theory of the low-frequency dielectric dispersion of colloidal particles in electrolyte solution. *J. Phys. Chem.* **66**, 2636–2642.

Selig, E. T. & Manuskhani, S. (1975). Relationship of soil moisture to the dielectric property. *J. Geotech. Engng, ASCE* **101**, GT8, 755–770.

Sen, P. N., Scala, C. & Cohen, M. H. (1981). A self-similar model for sedimentary rocks with application to the dielectric constant of fused glass beads. *Geophysics* **46**, No. 5, 781–795.

Sheeran, D. E. & Krizek, R. J. (1971). Preparation of homogeneous soil samples by slurry consolidation. *J. Mater. JMLSA* **6**, No. 2, 356–373.

Shirley, D. J. & Hampton, L. D. (1978). Shear-wave measurements in laboratory sediments. *J. Acoust. Soc. Am.* **63**, No. 2, 607–613.

Smith, M. C., Vellidis, G., Thomas, D. L. & Breve, M. A. (1992). Measurements of water table fluctuations in sandy soil using ground penetrating radar. *Trans. ASAE* **34**, No. 4, 1161–1166.

Sridharan, A. & Jayadeva, M. S. (1982). Double layer theory and compressibility of clays. *Géotechnique* **32**, No. 2, 133–144.

Thomann, T. G. & Hryciw, R. (1990). Laboratory measurement of small strain shear modulus under Ko condition. *ASTM Geotech. J.* **13**, No. 2, 97–105.

van Beek, L. K. (1967). Dielectric behavior of heterogeneous systems. In *Progress in dielectrics*, ed. J. B. Briks, Vol. 7, pp. 69–141. Cleveland, OH: CRC Press.

Viggiani, G. & Atkinson, J. H. (1995). Stiffness of fine-grained soils at very small strains. *Géotechnique* **45**, No. 2, 249–265.

von Hippel, A. R. (1954). *Dielectric and waves*, 1st student edn. Wiley.

Wang, J. R. (1980). The dielectric properties of soil–water mixtures at microwave frequencies. *Radio Science* **15**, No. 5, 977–985.

Wang, J. R. & Schmugge, T. J. (1980). An empirical model for the complex dielectric permittivity of soil as a function of water content. *IEEE Trans. Geosci. Remote Sensing* **GE 18**, 288–295.